Structural Comparison of Hydrogen Silsesquioxane Based Porous Low-*k* Thin Films Prepared with Varying Process Conditions

Hae-Jeong Lee,*,† Eric K. Lin,*,† Howard Wang,† Wen-li Wu,† Wei Chen,‡ and Eric S. Moyer‡

Polymers Division, National Institute of Standards and Technology, Gaithersburg, Maryland 20899, and Semiconductor Fabrication Materials, Dow Corning, Midland, Michigan 48640

Received November 12, 2001. Revised Manuscript Received January 31, 2002

The structures of hydrogen silsesquioxane based porous low dielectric constant (low-*k*) films (XLK) prepared with varying process conditions are characterized using a combination of high-energy ion scattering, X-ray reflectivity, and small-angle neutron scattering. We measure the film thickness, average mass density, density depth profile, wall density, porosity, average pore size, pore spacing, pore connectivity, and atomic composition. We compare samples with varying dielectric constants and degrees of cure or Si−H bonding fraction. The structural parameters are correlated with the chemical bond structure as measured by Fourier transform infrared spectroscopy. The density profiles of the porous films were uniform, with a slight densification observed at the film surface. Films with similar *k* values but varying degrees of cure have almost identical structural characteristics. Lower dielectric constant films have larger porosities and average pore sizes but lower wall densities. The process conditions used to alter the dielectric constant affect not only the porosity but also many other structural parameters such as the wall density.

Introduction

An ongoing challenge in semiconductor processing is the development of lower cost integrated circuits (ICs) with improved device performance. Improving device performance is primarily limited by signal delay through metal interconnects from the resistance, *R*, in the metal lines and the capacitance, *C*, between adjacent lines. This *RC* delay becomes more important when device dimensions in ICs shrink below 0.25 μm. There are two ways to reduce *RC* delay: lowering the resistance of the metal line and lowering the dielectric constant of the interlayer dielectric (ILD) material. Today, copper has replaced aluminum as the metal line material because of its low resistivity and high resistance to electromigration. On the dielectric side, many new ILD materials with low dielectric constants (low-*k*) are rapidly being developed to replace the current interlevel dielectric, silicon dioxide. *The National Technology Roadmap for Semiconductors* indicated a need for materials with dielectric constants of 2.0−2.5 in the year 2001 and materials with dielectric constants of 1.5−2.0 for dimensions below 0.13 μm by the year 2003.[1]

There are many choices for materials with dielectric constants larger than 2.5, including spin-coated organic polymers and silsesquioxanes, chemically vapor deposited (CVD) carbon- and fluorine-doped silicon oxide, and templated sol−gel silicas. The dielectric constants of these materials are generally lowered by incorporating chemical substituents such as hydrogen or alkyl groups and introducing bonds with low polarizabilities. However, this strategy cannot lower *k* below 2.2. Further decreases in the dielectric constant below 2.2 require the incorporation of air voids ($k = 1.01$) into a suitable dielectric matrix.[2,3] The development of new porous dielectric films has been very actively pursued, and several types of porous materials were reported.[4−8] Among several candidates of porous materials, hydrogen silsesquioxane (HSQ) based porous materials have been evaluated extensively because of their potential compatibility with conventional Si technology and the strength of the backbone siloxane network.[9,10] Although porous low-*k* materials can improve the IC performance, unlike nonporous low-*k* materials, the physical prestructure seriously affects other properties crucial to the integrated chip. The semiconductor industry requires pre-

† National Institute of Standards and Technology.
‡ Dow Corning.

(1) *The National Technology Roadmap for Semiconductors*; Semiconductor Industry Association: San Jose, CA, 1997.
(2) Morgen, M.; Ryan, E. T.; Zhao, J. H.; Hu, C.; Cho, T.; Ho, P. S. *Annu. Rev. Mater. Sci.* **2000**, *30*, 645.
(3) Nguyen, C. V.; Carter, K. R.; Hawker, C. J.; Hedrick, J. L.; Jaffe, R. L.; Miller, R. D.; Remenar, J. F.; Rhee, H. W.; Rice, P. M.; Toney, M. F.; Trollsas, M.; Yoon, D. Y. *Chem. Mater.* **1999**, *11*, 3080.
(4) Hawker, C. J.; Hedrick, J. L.; Miller, R. D.; Volksen, W. *Mater. Res. Soc. Bull.* **2000**, *25* (4), 54.
(5) Kondoh, E.; Asano, T.; Nakashima, A.; Komatu, M. *J. Vac. Sci. Technol. B* **2000**, *18*, 1276.
(6) Mikoshiba, S.; Hayase, S. *J. Mater. Chem.* **1999**, *9*, 591.
(7) Yang, H. S.; Choi, S. Y.; Hyun, S. H.; Park, C. G. *Thin Solid Films* **1999**, *348*, 69.
(8) Yang, S.; Mirau, P.; Pai, C. S.; Nalamasu, O.; Reichmanis, E.; Lin, E. K.; Lee, H. J.; Gidley, D. W.; Sun, J. N. *Chem. Mater.* **2001**, *13*, 2762.
(9) List, R. S.; Singh, A.; Ralston, A.; Dixit, G. *Mater. Res. Soc. Bull.* **1997**, *22* (10), 61.
(10) Aoi, N. *Jpn. J. Appl. Phys.* **1997**, *36*, 1355.

10.1021/cm011569h CCC: $22.00
Published on Web 03/28/2002

cise control over the structural characteristics of porous low-*k* thin films such as the porosity, pore size, and pore connectivity. It is essential to have methods to characterize the on-wafer structure of these porous thin films to understand and interpret correlations between processing conditions and the resulting physical properties. Currently, there are few experimental techniques able to characterize the porosity of thin films as prepared on a silicon substrate.[11−14]

In this work, we measure the structural properties of HSQ-based porous thin films (Dow Corning XLK[15]) prepared under a range of processing conditions using unique on-wafer measurements. The methodology employs a combination of ion scattering techniques, high-resolution specular X-ray reflectivity (SXR), and small-angle neutron scattering (SANS). We extract important structural information such as film thickness, the density depth profile, average pore size, pore spacing, pore connectivity, porosity, density of wall material between the pores, average mass density, and elemental composition. The influence of the processing conditions on the chemical bonding structure or degree of cure of the XLK films is also investigated using Fourier transform infrared (FTIR) spectroscopy. This methodology provides the unique determination of both the film porosity and wall density, two quantities that are difficult to separate using other measurement methods. In this way, we determine if lower dielectric constants arise primarily from increases in the film porosity (wall density constant) or if varying process conditions affects other structural parameters. We use two series of samples to investigate the influence of processing conditions on the structural characteristics of porous thin films. In one series, we compare samples with similar degrees of cure or Si−H bond fractions where the dielectric constant was varied from 1.5 to 2.2. In a second series of samples, we compare samples with the same dielectric constant while the Si−H fraction was varied from 30% to 52%.

Experimental Section

The films were prepared by spin-coating a solution containing a HSQ resin, a low boiling point solvent (methyl propyl ketone), and a high boiling point solvent (tetradecane) onto 200 mm silicon wafers. The solution composition for each sample is summarized in Table 1. Methyl propyl ketone is used to control the thickness of the as-spun film, and tetradecane functions as a porogen that is thermally removed to create voids or porosity in the dielectric film. The as-spun films undergo gelation through exposure to wet ammonia for 30−120 s at room temperature. After the wet ammonia treatment, the films are baked on a hot plate at 150 °C for 60 s under ambient atmosphere and cured in a furnace at 450 °C for 1 h in a low oxygen atmosphere (<10 ppm).[16,17] Increasing mass fractions of tetradecane solvent are used to lower the dielectric constant. Longer wet ammonia treatment times are applied to increase the degree of cure or the number fraction of Si−H of the films. The samples in this study are identified through both their dielectric constant and the Si−H fraction. The first two numbers in the sample name represent the dielectric constant, and the second two numbers represent the Si−H fraction. Thus, sample k20_47 has a dielectric constant of 2.0 and a Si−H bond fraction of 47%.

Table 1. Solution Composition for Each Sample

sample	dielectric constant	tetradecane wt %	methyl propyl ketone wt %	HSQ wt %
k15_42	1.5	23	57	20
k15_49	1.5	23	57	20
k20_30	2.0	14.6	66.4	19
k20_35	2.0	14.6	66.4	19
k20_47	2.0	14.6	67	19
k20_52	2.0	14.6	67	19
k22_51	2.2	12	67	21

The elemental compositions of the films were determined using Rutherford backscattering spectrometry (RBS) for silicon, carbon, and oxygen and forward recoil spectrometry for hydrogen. In both techniques, a beam of high-energy helium ions is directed toward the sample surface. The number of scattered or recoiled particles was counted as a function of energy.[18] The elemental composition of the film can be determined because the scattered energy is dependent upon the mass of each elemental species. The measurements were performed under vacuum from samples exposed to ambient atmospheric conditions, and fits were performed on the scattered peaks to compute the relative fraction of each element. The RBS analysis also provides the number of atoms per unit area. Given the thickness of the film, the RBS data can be used to determine the average mass density of the porous thin film.

SXR measurements were performed using a modified high-resolution X-ray diffractometer in a $\theta-2\theta$ configuration at the specular conditions with the incident angle equal to the detector angle. The instrument uses a tube source with fine-focus Cu Kα radiation having a wavelength, λ, of 1.54 Å. The incident beam was conditioned with a four-bounce germanium (220) monochromator. Before the detector, the beam was further conditioned with a three-bounce germanium (220) channel cut crystal. The goniometer has an active servo feedback system to provide an angular reproducibility of ±0.0001°. The data throughout the manuscript, in the figures, and in the tables are presented along with the standard uncertainty (±) involved in the measurement. This instrumental configuration enables the observation of interference fringes from films with thicknesses up to 1.2 μm. The reflected intensity was collected as a function of the grazing incident angle, and the measured angular range was 0.1−1.0°. SXR data are used to measure the thickness, average density, and density depth profile of the porous thin films.

SANS measurements were performed on the 8 m NG1 line at the National Institute of Standards and Technology Center for Neutron Research. The neutron wavelength was 6 Å with a wavelength spread (fwhm) $\Delta\lambda/\lambda$ of 0.14. The sample to detector distance was 3.6 m, and the detector was offset by 3.5° from the incident beam to increase the range of observable angles. The samples were placed in rectangular quartz cells with a 5 mm path length with the film surface perpendicular to the incident beam. To increase the scattered intensity from these thin films, up to six sample pieces were stacked. Two-dimensional scattering patterns were collected from the samples

(11) Gidley, D. W.; Frieze, W. E.; Dull, T. L.; Yee, A. F.; Nguyen, C. V.; Yoon, D. Y. *Appl. Phys. Lett.* **2000**, *76*, 1282.
(12) Dultsev, F. N.; Baklanov, M. H. *Electrochem. Solid State Lett.* **1999**, *2*, 192.
(13) Wu, W. L.; Wallace, W. E.; Lin, E. K.; Lynn, G. W.; Glinka, C. J.; Ryan, E. T.; Ho, H. M. *J. Appl. Phys.* **2000**, *87*, 1193.
(14) Kohdoh, E.; Baklanov, M. R.; Lin, E. K.; Gidley, D. W.; Nakashima, A. *Jpn. J. Appl. Phys.* **2001**, *40*, L323.
(15) Certain commercial equipment and materials are identified in this paper in order to specify adequately the experimental procedure. In no case does such identification imply recommendation by the National Institute of Standards and Technology, nor does it imply that the material or equipment identified is necessarily the best available for this purpose.
(16) Jin, C.; Wetzel, J. *Int. Interconnect Technol. Conf. (IITC) Proc.* **2000**, 99.
(17) Deis, T. A.; Saha, C.; Moyer, E.; Chung, K.; Liu, Y.; Spaulding, M.; Albaugh, J.; Chen, W.; Bremmer, J. *Mater. Res. Soc. Symp. Proc.* **2001**, *612*, D5.18.
(18) Tesmer, J. R.; Nastasi, M. *Handbook of Modern Ion Beam Materials Analysis*; Materials Research Society: Pittsburgh, PA, 1995.

Table 2. Elemental Composition and SXR Results of HSQ-Based Porous Thin Films after Varying Process Conditions[a]

sample	dielectric constant	Si−H fraction (%)	atomic composition (Si:O:C:H, %)	film thickness (Å)	q_c^2 ($\times 10^{-4}$) (Å^{-2})	wall density (g/cm^3)	average density (g/cm^3)		densified layer	
							SXR	RBS	thickness (Å)	density (g/cm^3)
k15_42	1.5	42	27:49:8:16	13 290	2.75	1.57	0.64	0.57	300	0.66
k15_49	1.5	49	28:49:8:15	13 270	2.71	1.65	0.63	0.58	260	0.64
k20_30	2.0	30	26:51:8:15	10 200	3.85	2.10	0.89	0.82	190	0.91
k20_35	2.0	35	25:49:9:17	7 780	3.77	2.02	0.87	0.81	200	0.89
k20_47	2.0	47	24:45:11:20	10 630	3.52	1.80	0.81	0.77	210	0.83
k20_52	2.0	52	26:49:6:19	7 940	3.58	1.98	0.83	0.74	260	0.87
k22_51	2.2	51	26:50:8:16	7 570	4.52	2.17	1.05	0.92	230	1.06

[a] The relative standard uncertainties of the atomic composition, film thickness, q_c^2, and density are ±5%, 10 Å, 0.05 Å^{-2}, and 0.05 g/cm^3, respectively.

for up to 6 h for sufficient count statistics. The two-dimensional data were corrected for empty quartz cell scattering, background scattering, detector uniformity, and sample thickness using standard reduction methods.[13] The scattered intensity was reduced to an absolute intensity scale with reference to a secondary water standard. The two-dimensional data were circularly averaged to produce one-dimensional data. Scattering measurements were performed under ambient conditions to determine the structural characteristics such as the average pore size of the pores in the films. Measurements were also made on samples immersed in deuterated toluene (toluene-d_8), a solvent that readily wets the sample. Changes in the scattered intensity after immersion in toluene-d_8 provide a measure of the percentage of pores that are interconnected and accessible to the film surface.

Infrared absorption spectra with wavenumbers ranging from 400 to 4000 cm^{-1} were recorded with a spectrometer with 4 ± 0.01 cm^{-1} spectral resolution. The data from each sample were averaged over 100 scans to increase the signal-to-noise ratio. The final sample spectra were obtained after subtracting the peaks due to the silicon substrate. The Si−H fractions were determined from the ratio of the area beneath the Si−H peaks in the as-spun and cured samples.

Results and Discussion

The use of several complementary experimental methods provides quantitative measurements of many porous thin film structural parameters. Some quantities require the use of only one method, but the unique determination of the porosity and the wall density requires information from all three experimental techniques. We first present the data from the SXR measurements of the average density, thickness, and depth profile of the films. Then, we show the SANS data of the average pore size and pore interconnectivity of the films. These measurements are combined with the elemental composition to determine the porosity and wall density of films prepared under varying process conditions. All of the elemental and structural data are summarized in Tables 2 and 3.

Figure 1 shows both the SXR data and the best fit to the data from a film with a dielectric constant of 2.0 and a Si−H fraction of 35%. The SXR data are plotted as the logarithm of the ratio of the reflected intensity to the incident beam intensity (I_r/I_0) or reflectivity versus the momentum transfer normal to the film, q. The momentum transfer is related to the incident angle of the X-ray beam, θ, through $q = (4\pi/\lambda) \sin \theta$. At low q values, the incident X-ray beam is nearly totally reflected from the sample surface and the reflectivity approaches unity. At angles larger than a critical angle, θ_c, the X-ray beam penetrates into the film, resulting in a sharp decrease in the reflectivity. The critical angle is proportional to the average electron density of the film through the equation $\theta_c = \lambda(\rho_e r_e/\pi)^{1/2}$, where ρ_e is the electron density and r_e is the classical electron radius, 2.818 fm. Given the elemental composition of the film, the electron density is easily converted into an average mass density. For the film in Figure 1, the electron density from the critical angle of the film is 0.266 ± 0.005 e/Å^3, with a resulting average mass density of 0.87 ± 0.01 g/cm^3. The average mass density of the film is related to the porosity and wall density of the film through a rule of mixtures

$$\rho_{ave} = \rho_w(1 - P) \quad (1)$$

where ρ_w is the density of the wall material between the pores and P is the porosity of the film. A second

Table 3. Structural Properties of HSQ-Based Porous Thin Films after Varying Process Conditions[a]

sample	dielectric constant	Si−H fraction (%)	pore size (Å)	pore spacing (Å)	porosity (%)
k15_42	1.5	42	40	27	60
k15_49	1.5	49	41	25	62
k20_30	2.0	30	30	22	57
k20_35	2.0	35	30	23	57
k20_47	2.0	47	27	22	55
k20_52	2.0	52	26	19	58
k22_51	2.2	51	21	20	52

[a] The relative standard uncertainties of pore size, pore spacing, and porosity are ±1 Å, 1 Å, and 5%, respectively.

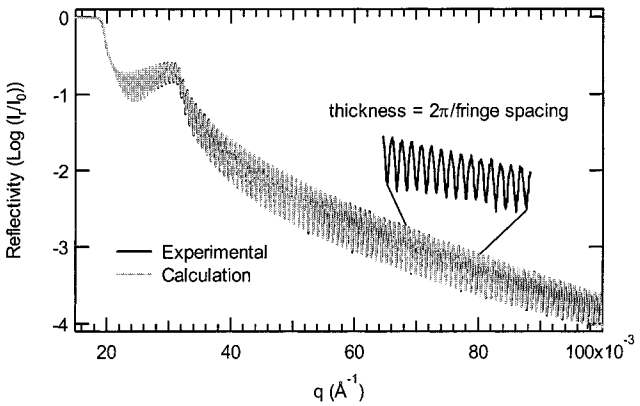

Figure 1. SXR curve of HSQ-based porous thin films with a dielectric constant of 2.0 and a Si−H fraction of 35%. Those are presented as the logarithm of the ratio of the reflected beam intensity (I_r) to the incident beam intensity (I_0) versus the magnitude of the momentum transfer in the film thickness direction (q). The black and gray curves represent the experimental and calculated data, respectively. The inset shows fringes ranging from 0.068 to 0.080 Å^{-1}, used to calculate the film thickness.

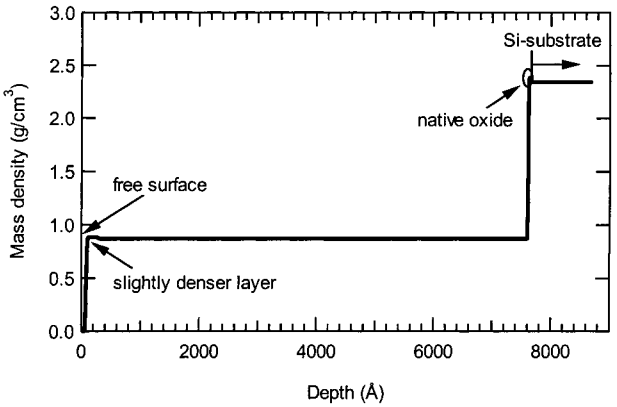

Figure 2. Calculated electron density depth profile of the film in Figure 1. The free surface is located at the far left of the horizontal axis, and the silicon substrate is located at the far right of the abscissa.

critical angle is observed in the data at slightly higher q values and is due to the silicon substrate.

If the densities of the thin films are different from that of the substrate, interference oscillations are observed in the reflectivity profile. The periodicity of the interference fringes is determined by the overall thickness of the film. At high enough q values, the film thickness, t, can be determined from the period of the oscillations, Δq, through the relationship $t = 2\pi/\Delta q$, because multiple scattering contributions to the reflectivity signal are less than 1% of the reflected intensity.[13,19] Here, the thickness of porous thin films was determined from the periodicity of the fringes within a q range of 0.068−0.080 Å^{-1}. The thickness of the film in Figure 1 is 7780 ± 10 Å.

To determine the density depth profile of the films, the SXR data are fitted to model electron density profiles using a least-squares fitting routine based upon the algorithm of Parratt.[20] Model profiles with several layers having variable thickness, electron density, and roughness are numerically adjusted until the calculated reflectivity agrees with the experimental data. The theoretical basis of the deconvolution of the SXR data is described in detail elsewhere.[20] Figure 1 shows the excellent agreement between the calculated and experimental data. Figure 2 shows the electron density depth profile corresponding to the best fit to the SXR data in Figure 1. The depth profile is uniform with a thin, denser layer at the free surface of the film. The thickness of the dense layer is 200 ± 10 Å, and the electron density of this layer is approximately 1% higher than that of the bulk layer. A native oxide layer approximately 50 Å thick was also detected between the porous low-k film and the silicon surface. The measurement of these subtle density differences illustrates the sensitivity and resolution of the SXR technique.

Two layers are sufficient to fit adequately the experimental data in this study. However, in an earlier publication, four distinct layers were needed to fit the reflectivity data from standard HSQ films.[21] These

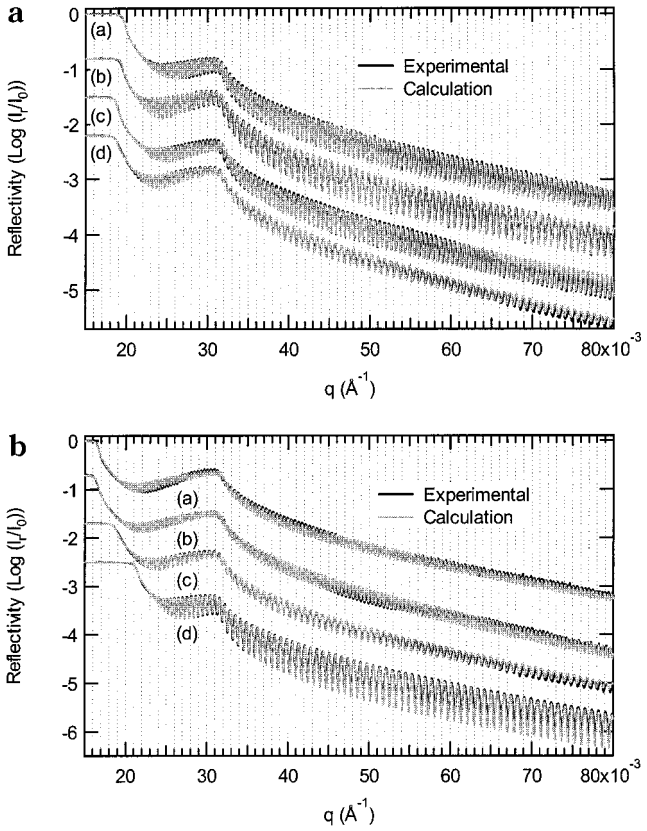

Figure 3. SXR curves of HSQ-based porous thin films with a a dielectric constant of 2.0 and different Si−H fractions of (a) 30%, (b) 35%, (c) 47%, and (d) 52% and b a similar range of Si−H fractions ranging from 49% to 51% and different dielectric constants of (b) 1.5, (c) 2.0, and (d) 2.2. The SXR curve of a film with a dielectric constant of 1.5 and a Si−H fraction of 42% is also shown in part b (a) as a comparison to a film with a dielectric constant of 1.5 and a Si−H fraction of 49%. Curves are offset for clarity.

differences in the homogeneity of the density profiles are most likely due to differences in the bake process used to prepare the two types of HSQ. The standard HSQ film preparation uses three sequential bake steps at 150, 200, and 350 °C. The porous HSQ films preparation uses only one bake step at 150 °C and a curing step at 450 °C. The bake process in the ambient atmosphere densifies the top surface of the film dense through oxidation by atmospheric oxygen. The three separate bake steps used during the HSQ process are at higher temperatures and result in more complicated density profiles from successive densification of the HSQ film.

The data and best fits to the SXR data from samples with the same k value but a different Si−H fraction are shown in Figure 3a, and those from samples with similar Si−H fractions and different k values are shown in Figure 3b. For films with lower dielectric constants, the first critical angle moves to lower q values, indicating that films with lower k have a lower average density. Also, the data from films with lower dielectric constants and films with higher Si−H fractions have oscillations with smaller amplitudes and more rapidly decreasing reflectivities. These features are characteristic of increasing film roughness because the specular reflectance at angles beyond the critical angle decreases faster than those values calculated for an ideal smooth interface

(19) Bouldin, C. E.; Wallace, W. E.; Lynn, G. W.; Roth, S. C.; Wu, W. L. *J. Appl. Phys.* **2000**, *88*, 691.
(20) Parratt, L. G. *Phys. Rev.* **1954**, *95*, 359.
(21) Lee, H. J.; Lin, E. K.; Wu, W. L.; Fanconi, B. M.; Liou, H. C.; Lan, J. K.; Cheng, Y. L.; Wang, Y. L.; Feng, M. S.; Chao, C. G. *J. Electrochem. Soc.* **2001**, *148*, F195.

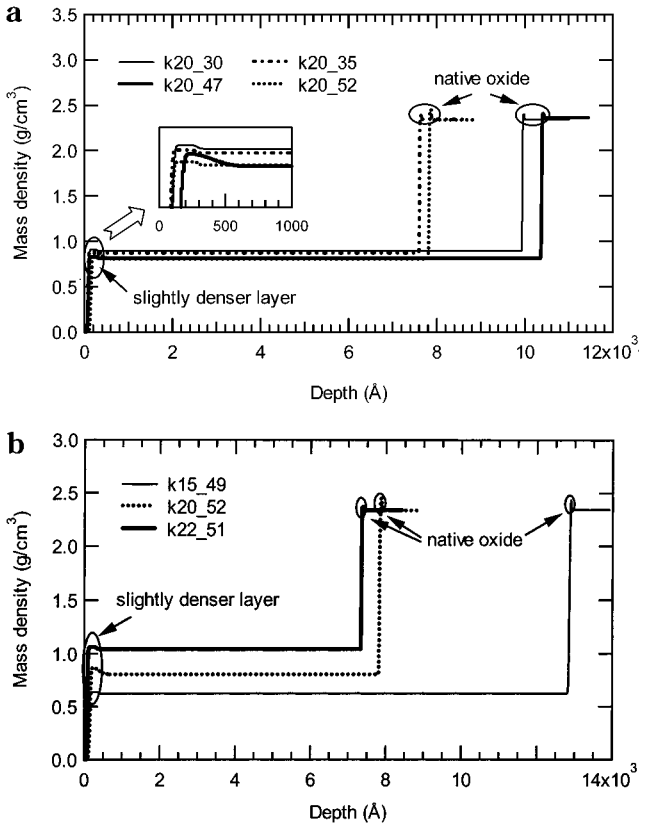

Figure 4. Electron density depth profiles of the films in Figure 3. a Films with a dielectric constant of 2.0 and different Si−H fractions of 30%, 35%, 47%, and 52%. The inset shows clearly the region of a slightly denser layer from the free surface to the depth of 1000 Å. b Films with a similar range of Si−H fractions ranging from 49% to 51% and different dielectric constants of 1.5, 2.0, and 2.2.

using the Fresnel equations.[22,23] Parts a and b of Figure 4 show the mass density depth profiles corresponding to the best fits to the data in Figure 3. The mass density is directly calculated from the electron density and elemental composition. The elemental composition is uniform throughout the film (from RBS measurements). Figure 4a and Table 2 show that changes of the Si−H fraction do not significantly change the average density of the films. This suggests that changes in the chemical structure or degree of cure of the HSQ network from the wet ammonia treatment may not significantly affect the modulus or other physical properties related to the film density. However, these chemical differences may affect other important properties such as the amount of moisture absorption in the film.

In Figure 4a, denser surface layers of films are observed in films with the same dielectric constant and varying Si−H fraction. The thickness of the denser layer increases slightly with increasing Si−H fraction and decreasing dielectric constant, but the values are similar, ranging from 190 to 300 Å in thickness. The densities of these layers are only 1−5% greater than those of the bulk layer. Native silicon oxide layers ranging from 40 to 60 Å in thickness were also measured in these films. The average mass densities of the

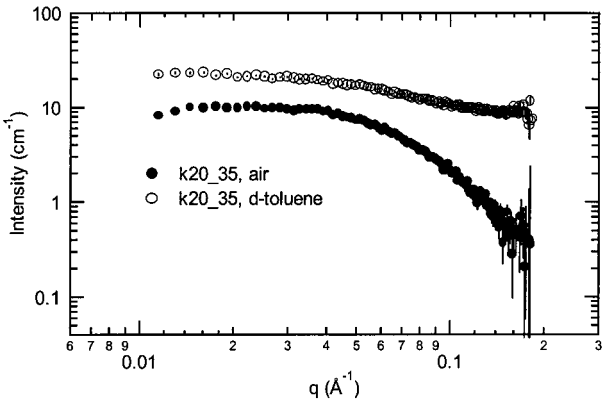

Figure 5. SANS data of the film with a dielectric constant of 2.0 and a Si−H fraction of 35% under ambient air conditions (filled symbols) and immersed in deuterated toluene (open symbols). Some error bars at the low q ranges are within the symbols.

films with dielectric constants of 2.2, 2.0, and 1.5 are approximately 1.05, 0.85, and 0.64 g/cm^3, respectively. These values are all significantly lower than the density of standard HSQ films (1.4−1.5 g/cm^3).[17] As a self-consistent check, the SXR average mass densities are found to be in good agreement, within experimental error, with the values determined from the RBS measurements. These trends are quantified in Table 2. At this point, the porosity of the porous XLK films may be estimated after assuming that the wall density of the film is equal to the density of the standard HSQ film. However, subsequent measurements with SANS will show differences in the wall density of the films from varying process conditions.

Figure 5 shows the SANS intensity from a porous film with a dielectric constant of 2.0 and a Si−H fraction of 35% both in an ambient air atmosphere and immersed in toluene-d_8 as a function of q, where $q = (4\pi/\lambda)\sin(\theta/2)$ and θ is the scattering angle. The scattering intensity of the air sample arises from differences in the neutron scattering length of connecting wall material and the pores. The SANS data are analyzed using a modification of the random two-phase model of Debye et al.[24] to a three-phase model.[25] In the three-phase model, the hydrogen and carbon within the film are assumed to segregate primarily to the pore surfaces. This assumption is needed because of the unique contrast hydrogen provides to neutrons. The scattering length density of hydrogen is negative, while those of silicon, carbon, and oxygen are positive. As a result, any segregation of hydrogen can result in an enhanced SANS intensity and unphysical values of the wall density. Assuming that carbon and hydrogen segregate to the pore surfaces, the SANS data may be analyzed using the two-phase Debye to determine the correlation length and the wall density and porosity may be determined with equations presented earlier.[25] The two- and three-phase versions of the Debye model provide limiting values on the wall density and porosity of the porous thin films.

In the Debye model, the density of the wall material between the pores is assumed to be uniform and the

(22) Lodha, G. S.; Yamashita, K.; Kunieda, H.; Tawara, Y.; Yu, J.; Namba, Y.; Bennett, J. M. *Appl. Opt.* **1998**, *37*, 5239.
(23) Santucci, S.; Cecilia, A. V. L.; Phani, A. R.; Alfonsetti, R.; Moccia, G.; Biase, M. D. *Appl. Phys. Lett.* **2000**, *76*, 52.
(24) Debye, P.; Anderson, H. R.; Brumberger, H. *J. Appl. Phys.* **1957**, *28*, 679.
(25) Wu, W. L.; Lin, E. K.; Jin, C.; Wetzel, J. T. *Mater. Res. Soc. Symp. Proc.* **2001**, *612*, D4.1.

density correlation function describing the porous structure is assumed to be exponential through $\gamma(r) = \exp(-r/\xi)$, where ξ is the correlation length. The form of the scattered intensity is given by the equation

$$I(q) = \frac{8\pi P(1-P)\Delta\rho_n{}^2\xi^3}{(1+q^2\xi^2)^2} \quad (2)$$

where P is the porosity and $\Delta\rho_n$ is the neutron scattering contrast, a function of ρ_w. Equation 2 well describes the scattering data over the accessible angular range of the instrument. The correlation length, ξ, can be determined from an extrapolation of the experimental data to $q = 0$. Once ξ is known, eq 2 becomes a function only of P and ρ_w. Similarly, eq 1 from the SXR and RBS measurements provides another relationship between ρ_w and P. Equations 1 and 2 can be solved to determine uniquely the average wall density and porosity. Additionally, the average chord length, l_c, a measure of the average pore size, is given by the equation $l_c = \xi/(1-P)$. For the sample shown in Figure 5, the porosity was determined to be 57 ± 5% and the wall density was 2.02 ± 0.05 g/cm^3. Given the porosity, the average pore size is 30 ± 1 Å. The structural parameters for all of the samples are calculated in the same way and summarized in Table 3.

In Figure 5, the scattering intensity is significantly stronger for the film immersed in toluene-d_8 than in air. The relatively high neutron cross section of toluene-d_8 significantly enhances the scattering intensity. If all of the pores are connected and open to the solvent through the film surface and given the neutron scattering density for toluene-d_8, the scattering contrast is enhanced by a factor of 18.3. The fraction of pores that are interconnected and accessible to the film surface can be estimated from the magnitude of the increase in the scattering intensity. For all of the films in this study, the pores were fully interconnected.

Figure 6a shows the SANS data from samples with the same dielectric constant and varying Si−H fraction, and Figure 6b shows the SANS data from samples with different dielectric constants and similar Si−H fractions. The SANS intensity from the data in Figure 6a are nearly identical, with slightly lower scattering from samples with higher Si−H fractions. From Figure 6b, the scattering intensity of the film with a dielectric constant of 1.5 is much higher than those from films with dielectric constants of 2.0 and 2.2. In general, the increased scattered intensity indicates that the lower dielectric constant films have larger porosities and/or average pore sizes. The quantitative values of the structural parameters of these films are shown in Table 3. When the dielectric constant decreases from 2.2 to 1.5, the wall density decreases from 2.17 ± 0.05 to 1.57 ± 0.05 g/cm^3, the porosity increases from 52 ± 5% to 62 ± 5%, and the average pore size increases from 21 ± 1 to 40 ± 1 Å. The average pore spacing (ξ/P) or chord length of the wall material varies between 20 ± 1 and 27 ± 1 Å. For a given dielectric constant material, the average mass density, wall density, pore size, and porosity generally decrease with increasing Si−H fractions, but the changes are small (less than 10% change). The wall densities of the porous films are generally

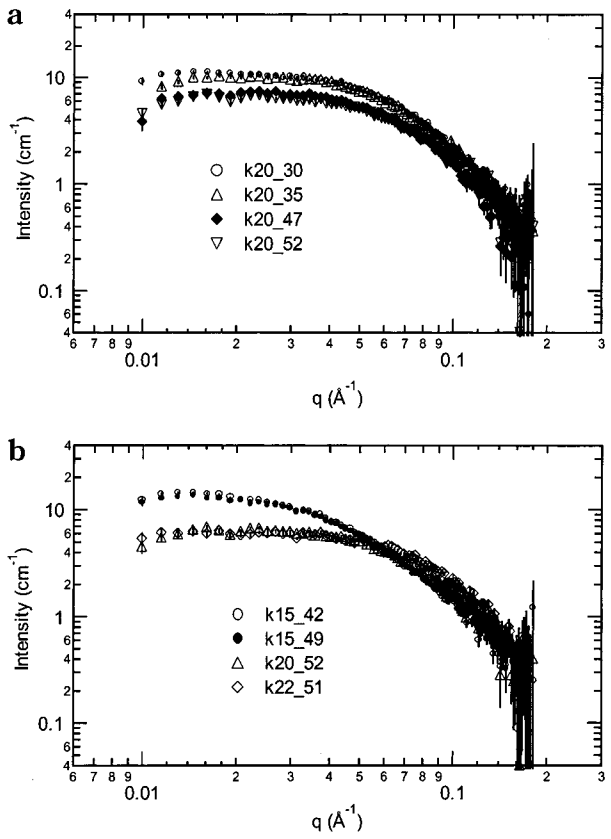

Figure 6. SANS data of HSQ-based porous thin films with a, a dielectric constant of 2.0 and different Si−H fractions of 30%, 35%, 47%, and 52% and with b a similar range of Si−H fractions ranging from 49% to 51% and different dielectric constants of 1.5, 2.0, and 2.2. The SANS results of a film with a dielectric constant of 1.5 and a Si−H fraction of 42% are also shown in part b as a comparison to a film with a dielectric constant of 1.5 and a Si−H fraction of 49%. Error bars at the low q range are smaller than the symbols.

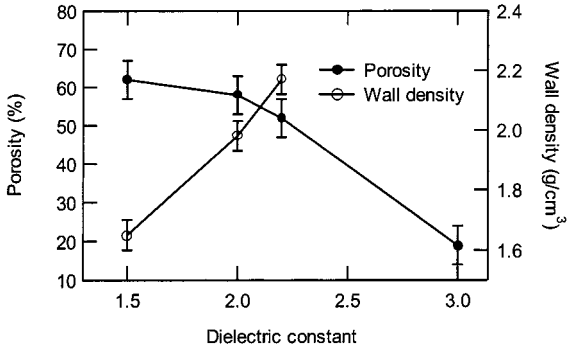

Figure 7. Porosity and wall density shown as a function of the dielectric constant. The k value from a standard HSQ is also shown for comparison. The solid lines are solely intended to emphasize trends in the experimental data.

higher than those of standard HSQ films (1.4−1.5 g/cm^3) but lower than those of thermal oxides grown on a silicon wafer (2.27 g/cm^3).

These detailed measurements provide insight into correlations between the porous film structure and the dielectric constant and the formation process of the porous thin films. Lower dielectric constant films have larger pores because larger fractions of the high boiling point solvent used as the pore generator are used in the initial solution. However, as shown in Figure 7, the differences in porosity between films with dielectric

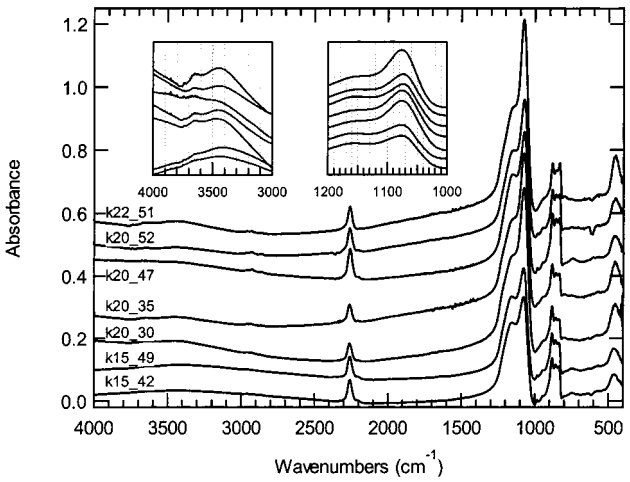

Figure 8. FTIR spectra of HSQ-based porous thin films with different process conditions presented as the relative intensity of absorbance versus wavenumber. The inset shows clearly the differences of the Si−O stretching peak position in the range of 1000−1200 cm^{-1} and Si−OH peaks in the range of 3000−4000 cm^{-1}. Curves are offset vertically for clarity.

constants of 1.5 and 2.2 are not large. The data for pure HSQ with a dielectric constant of 3.0 is also shown in the figure for comparison.[26] Decreases in the dielectric constant are due to both slight increases in the porosity and significant decreases in the wall density. An alternative interpretation may be that the effect of the high boiling point solvent at larger mass fractions is to create more microporosity (pores < 5 Å) rather than mesoporosity (pores > 10 Å). The SANS measurements are not sensitive to microporosity because the probing wavelength is 6 Å. Here, microporosity and decreased wall densities are not distinguishable.

The changes in the wall density can also be correlated with changes in the HSQ network bonding structure using FTIR measurements. During the gelation process under a wet ammonia atmosphere, the cages and Si−H bonds in the HSQ resin are cleaved and transformed into a dense SiO_2 network structure. These changes may be monitored by measuring the peak widths, shifts, and moisture absorption at wavenumbers corresponding to Si−O−Si stretching modes and to moisture absorption or Si−OH bonds. In general, SiO_2-like spectra and increased moisture absorption are signatures of denser Si−O network wall materials. The porous films studied here all have wall densities that fall between those of the standard HSQ resin and thermally grown SiO_2. The wall density, however, increases with increasing dielectric constant and decreasing Si−H fraction consistent with differences in the wall HSQ network structure for each particular film. These observations are consistent with FTIR results shown in Figure 8. The ν_{as}(Si−O−Si) asymmetric stretching modes near 1132−1136 cm^{-1} due to the initial HSQ cage structure broaden with decreasing Si−H fraction and increasing dielectric constant. Another ν_{as}(Si−O−Si) peak near 1072−1076 cm^{-1} due to the Si−O bonds in the cured network structure shifts to higher wavenumbers with decreasing Si−H fraction and increasing dielectric constant. These peak positions are higher than those from standard HSQ films at 1068 cm^{-1} but lower than those from silicon oxide. This indicates that more Si−H bonds in the HSQ resin are converted into Si−O bonds in the porous thin films than in standard HSQ films.[27] Additionally, these electronegative oxygen atoms effectively attract electrons away from neighboring Si−O bonds, resulting in an increased Si−O bond strength or bond energy.[28,29] Finally, during bond cleavage of the HSQ resin during gelation, dangling bonds from the Si are generated, resulting in increased moisture absorption. The FTIR peak due to adsorbed water molecules and Si−OH bonds appears around 3300−3700 cm^{-1}. These peaks are stronger for samples with larger dielectric constants, lower Si−H fractions, and larger wall densities, as shown in the inset of Figure 8. These results show that an increase in the mass fraction of the high boiling point solvent in the initial solution changes not only the porous structure but also the chemical structure of the cured HSQ wall material.

Summary

We have applied a nondestructive methodology utilizing information from high-energy ion scattering, high-resolution SXR, and SANS to measure important structural and physical properties of HSQ-based porous thin films (XLK) prepared with different processing conditions. The structural measurements are detailed enough to provide important insight into correlations between the structure of the porous thin films and processing parameters. We prepared two different series of samples by varying either the time of wet ammonia treatment or the mass fraction of the high boiling point solvent in the initial resin solution. One series of samples has the same dielectric constant but varying degrees of cure or Si−H fractions. The other series has similar Si−H fractions but different dielectric constants. Combining the information from three measurement techniques, we measure the film thickness, electron density depth profile, average film density, matrix material density, porosity, average pore size, average pore spacing, pore connectivity, and atomic composition. This methodology uniquely provides measurements of both the porosity and wall density, quantities that are needed to better understand the dependence of the pore structure formation on the process conditions.

SXR measurements show that the porous films have very uniform density profiles. Only two layers are required to fit the SXR data. The top layer, approximately 190−300 Å thick, is slightly denser than the rest of the porous thin film. The average mass density and wall density of these films increase with increasing dielectric constant and decreasing Si−H fraction. When the dielectric constant decreases from 2.2 to 1.5, the wall density decreases from 2.17 ± 0.05 to 1.57 ± 0.05 g/cm^3, the porosity increases from 52 ± 5% to 62 ± 5%, and the average pore size increases from 21 ± 1 to 40 ± 1 Å. With increasing mass fractions in the resin solution, the high boiling point solvent not only increases the porosity but also decreases the wall material density.

(26) Liou, H. C.; Pretzer, J. *Thin Solid Films* **1998**, *335*, 186.

(27) Loboda, M. J.; Grove, C. M.; Schneider, R. F. *J. Electrochem. Soc.* **1998**, *145*, 2861.

(28) Agaskar, P. A.; Day, V. W.; Klemperer, W. G. *J. Am. Chem. Soc.* **1987**, *109*, 5554.

(29) Lucovski, G.; Yang, J.; Chao, S. S.; Tyler, J. E.; Czubatyj, W. *Phys. Rev. B* **1983**, *28*, 3225.

These density changes reflect differences in the degree of conversion of the HSQ resin into a SiO_2-like network. The films with larger wall densities such as those with a dielectric constant of 2.2 or a Si−H fraction of 30% show higher Si−O bond energies and a peak-related water absorption in FTIR spectra. These results represent the first data to characterize the effects of a solvent-based porogen and process conditions on the wall density, porosity, and density depth profile. The detailed quantitative measurements presented here demonstrate unique information that may be used by the semiconductor industry and materials scientists to better control process conditions and design new materials for enhanced IC fabrication and performance.

CM011569H